PAPER

Reaction mechanism from quantum molecular dynamics for the initial thermal decomposition of 2,4,6-triamino-1,3,5-triazine-1,3,5-trioxide (MTO) and 2,4,6-trinitro-1,3,5-triazine-1,3,5-trioxide (MTO3N), promising green energetic materials†

Cai-Chao Ye,[ab] Qi An,[a] Tao Cheng,[a] Sergey Zybin,[a] Saber Naserifar,[a] Xue-Hai Ju[b] and William A. Goddard III[*a]

Klapötke and co-workers recently designed two new materials, 2,4,6-triamino-1,3,5-triazine-1,3,5-trioxide (**MTO**) and 2,4,6-trinitro-1,3,5-triazine-1,3,5-trioxide (**MTO3N**), envisioned as candidates for green high-energy materials. However, all attempts at synthesis have failed. In order to validate the expected properties for these systems and to determine why these materials are too unstable to synthesize, we used the PBE flavor of Density Functional Theory (DFT) to predict the crystal structures for **MTO** and **MTO3N** and then we carried out DFT molecular dynamics simulations (DFT-MD) to determine the initial reaction mechanisms for decomposition. Klapötke estimated that **MTO** would have a density of $\rho = 1.859$ g cm^{-3} with an estimated detonation velocity (D_v) of 8.979 km s^{-1}, making it comparable to RDX ($\rho = 1.82$ g cm^{-3}, $D_v = 8.75$ km s^{-1}) and β-HMX ($\rho = 1.91$ g cm^{-3}, $D_v = 9.10$ km s^{-1}). His estimated impact sensitivity >30 J, make it much better than HMX (7 J) and RDX (7.5 J). Our predicted crystal structure for **MTO** ($P2_{(1)}$ space group) leads to $\rho = 1.859$ g cm^{-3}, in good agreement with expectations. Our DFT-MD studies find that the first step in the decomposition of **MTO** is intermolecular hydrogen-transfer reaction (barrier 3.0 kcal mol^{-1}) which is followed quickly by H$_2$O and NO release with reaction barriers of 46.5 and 35.5 kcal mol^{-1}. In contrast for **MTO3N** ($P2_{(1)}/c$ predicted space group), we find that the first steps are a bimolecular decomposition to release NO$_2$ ($\Delta H = 44.1$ kcal mol^{-1}, $\Delta G = 54.7$ kcal mol^{-1}) simultaneous with unimolecular NO$_2$ cleavage ($\Delta H = 59.9$ and $\Delta G = 58.2$ kcal mol^{-1}) a unique initial reaction among EMs. These results suggest that **MTO3N** would be significantly more thermally stabile (barrier > 6.0 kcal mol^{-1} higher) than RDX and HMX, making it an excellent candidate to be insensitive new green energetic materials. However we find that **MTO** leads to very favorable hydrogen transfer reactions that may complicate synthesis and crystallization, making **MTO3N** the more promising system.

1. Introduction

Environmental concerns about current energetic materials (EM) make the development of green EM a high priority.[1] Moreover developing safe and efficient high-energy content materials is of vital importance to utilization in civil applications as propellants in satellite launch rockets, satellite propulsions system, and naval systems.[1,2] An ideal green explosive should have

[a]*Materials and Process Simulation Center, California Institute of Technology, 139-74, Pasadena, California 91125, United States. E-mail: wag@wag.caltech.edu*

[b]*Key Laboratory of Soft Chemistry and Functional Materials of MOE, School of Chemical Engineering, Nanjing University of Science and Technology, Nanjing 210094, P. R. China*

† Electronic supplementary information (ESI) available: Atomic coordinates of all intermediates and TSs shown in this study, coordinates for structures of $P2_{(1)}$-**MTO** and $P2_{(1)}/$c-**MTO3N**, and the bond cut-off in the fragment analysis. See DOI: 10.1039/c5ta02486b

higher velocity of detonation, higher detonation pressure, higher density, and lower sensitivity than benchmark explosives, such as RDX and HMX. Simultaneously it is important that the end products from detonation or combustion are environmentally friendly and that the syntheses not yield toxic or non-green materials that must be disposed. For this reason Klapötke *et al.* designed 2,4,6-triamino-1,3,5-triazine-1,3,5-trioxide (**MTO**) and 2,4,6-trinitro-1,3,5-triazine-1,3,5-trioxide (**MTO3N**) as potential new green energetic materials and estimated that velocity of detonation would be 8.979 km s^{-1} (compare to 8.855 km s^{-1} for RDX and 9.247 km s^{-1} for β-HMX) with density is 1.9 g cm^{-3} and impact sensitivity > 30 J, much better than HMX (7 J) and RDX (7.5 J).[3]

However, numerous attempts to synthesize **MTO** and **MTO3N** have not yet been successful. In order to predict more accurately the properties and to understand the stability, we recently predicted[4] the crystal packing and cohesive energy of
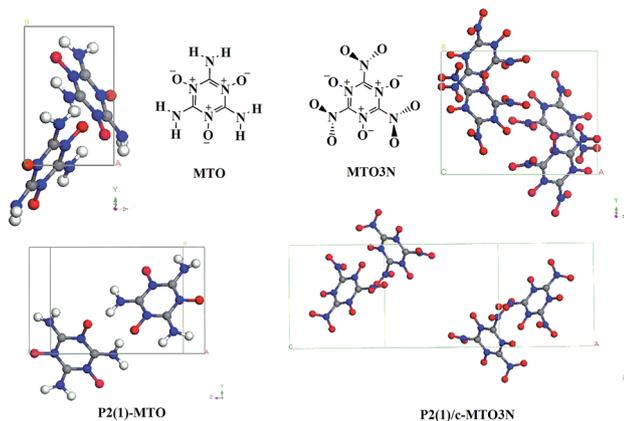
Fig. 1 2,4,6-Triamino-1,3,5-triazine-1,3,5-trioxide (**MTO**) and 2,4,6-trinitro-1,3,5-triazine-1,3,5-trioxide (**MTO3N**) molecular structures and their most stable crystal structures: $P2_{(1)}$ for **MTO** and $P2_{(1)}/c$ for **MTO3N** predicted from previous PBE DFT calculations.[4] The C, O, N, H atoms are represented by grey, red, blue and white balls, respectively.

MTO and **MTO3N** using Monte Carlo simulated annealing methods[5] with the PBE flavor of Density functional Theory[6] (DFT) (including the low gradient London dispersion correction)[7] (PBE-ulg) to find that **MTO** has the $P2_{(1)}$ space group with 2 molecules per cell and a density of 1.859 g cm^{-3}, while **MTO3N** has the $P2_{(1)}/c$ space group with 4 molecules per cell and a density of 2.016 g cm^{-3}. The two molecules and crystal structures are shown in Fig. 1.

In order to determine the energy release, detonation properties, and sensitivity of EMs, it is essential to determine the reaction mechanism for the initial steps leading to thermal decomposition.[8–14] For such nitro-based EMs as TNT, RDX, HMX and CL-20, the initial decomposition at low pressure is unimolecular NO_2 cleavage.[15–20] However for hydrogen containing highly energetic materials such as RDX and HMX, Chakraborty *et al.*[8,14,21] used DFT to show that intramolecular hydrogen transfer to form HONO provides a competitive first step for decomposition[22–27] that dominates under high impact conditions.[28] Since **MTO** has no –NO_2 group available to cleave off NO_2, and **MTO3N** has no hydrogen available to form HONO, their decomposition properties should be dramatically different (maybe better) than normal nitro-based explosives.

In this paper, we report the initial thermal decomposition reaction mechanisms of **MTO** and **MTO3N** using molecular dynamics simulations based on the PBE-ulg[7] flavor of DFT. The PBE-ulg corrects the poor description of van der Waals attraction (London dispersion) in PBE.[7] Here we consider **MTO** and **MTO3N** starting with their predicted most stable crystal structures ($P2_{(1)}$ for **MTO** and $P2_{(1)}/c$ for **MTO3N**).

2. Methodology

2.1. Quantum molecular dynamics simulation

In these DFT based molecular dynamics (MD) simulations, the interatomic forces were calculated in the framework of DFT,[29,30] where exchange and correlation were treated with the

generalized gradient approximation (GGA), using the PBE-ulg functional form.[7]

The periodic DFT calculations were performed using the VASP package.[31–34] For structure optimization we found that a kinetic energy cut-off of 500 eV for the plane wave expansions gives excellent convergence of the total energies, energy differences, and structural parameters. The same energy cut-offs were used in the DFT-MD calculations. Reciprocal space was sampled with the Γ-centered Monkhorst–Pack scheme using only the gamma point for the supercell calculations. The convergence criteria were set to a 1×10^{-6} eV energy difference for solving the electronic wave function and a 1×10^{-3} eV Å^{-1} force for geometry optimization. They were set to 1×10^{-5} eV energy difference for solving the electronic wave function and a 1×10^{-3} eV Å^{-1} force for DFT-MD simulation.

Two crystalline phases (**MTO**: $P2_{(1)}$ and **MTO3N**: $P2_{(1)}/c$) were considered in the DFT-MD simulations. The MD considered 8 molecules per periodic cell, obtained by replicating the unit cell twice along the "*a*" and "*b*" directions for **MTO** and replicating the unit cell twice along the "*c*" direction for **MTO3N**. Then the structures for the supercells were optimized individually before molecule dynamics simulations. The two initial structures of **MTO-$P2_{(1)}$** and **MTO3N-$P2_{(1)}/c$** are shown in Fig. S1.†

The procedure for the DFT-MD cook-off simulations was as follows: first the systems were heated from 20 K to 300 K over a period of 2 ps and then equilibrated at 300 K for 1 ps using the NVT (constant volume, constant temperature and constant number of atoms) ensemble. Finally, we heated the system from 300 K to 3000 K uniformly over the period of 20 ps, but with the volume fixed. The time constant for the Nose–Hoover thermostat was set to 0.1 ps. We used a time step of 1 fs for integrating the equations of motion. To analyse the fragments during the simulation, we used a bond length cut-off of 1.5 times of the normal bond length, as are shown in the Table S1.†

2.2. Finite cluster calculation

To analyse the mechanisms for the reactions discovered during the periodic DFT-MD simulations, we extracted the molecule structures involved (generally bimolecular) in the reaction from the periodic DFT-MD trajectories and then carried out finite molecule calculations to locate the nearby transition state (TS) for gas phase reactions at the level of M06/6-311++G** using the Jaguar program.[35] The TS's were validated to have only one negative eigenvalue for the Hessian. This was followed by intrinsic reaction coordinate (IRC) scans to connect the TS to nearby reactant and the product structures.[36] To obtain free energies, we diagonalized the mass reduced Hessian to obtain the vibrational frequencies, with which we evaluated the thermodynamic properties at 298.15 K and 1 atm. All gas phase calculations were carried out using the Jaguar 8.2 package.[35]

3. Results and discussion

These DFT-MD simulations provide a very detailed, molecular-level description of the decomposition and reactions of **MTO** and **MTO3N** in the condensed phase. This information allows

This journal is © The Royal Society of Chemistry 2015

J. Mater. Chem. A, 2015, **3**, 12044–12050 | **12045**

us to extract valuable information about the complex chemistry involved, including uni- and multi-molecular reactions.[12] Our goal is to elucidate the reaction pathway as **MTO** and **MTO3N** decomposes and evolves to form intermediates that react with each other and with reactant to form eventually the final products observed theoretically and presumably experimentally. In this work, we focus on thermal decomposition of condensed phase **MTO** and **MTO3N** crystals, examining the initial reaction pathways to evaluate the stability of these two promising green energetic materials.

3.1. MTO initial reaction

3.1.1. Quantum molecular dynamics simulation.
We first examined the initial decomposition reaction of $P2_{(1)}$-**MTO**. The molecular fragments during the cook-off simulation are plotted in Fig. 2 as a function of temperature. The starting supercell consists of 8 **MTO** molecules (144 atoms). We see that

1. No reactions are observed from 0 to 7 ps (up to 1250 K).

2. Simultaneous intermolecular H transfer between two **MTO** monomers is observed during the period 7 to 11 ps (up to 1700 K) to form the dimer containing adjacent NH and N–OH groups in place of NH_2 and $N–O^-$, with a structure similar to **TS1** in Fig. 3.

3. Then, at 11.5 ps ($\sim$1800 K) the first reaction occurs, a unimolecular reaction involving the intermediate formed in step 2 in which an NH_2 transfer a hydrogen to the N–OH group to release H_2O, leaving behind **INT2** (Fig. 3) with an opened ring.

4. Later at 13 ps ($\sim$2050 K), the first NO molecule is released from **INT2**.

Thus, we find that the unimolecular H_2O release subsequent to H transfers between two monomers is the initial decomposition reaction for $P2_{(1)}$-**MTO**. We will discuss these reaction mechanisms in more detail using finite cluster calculations. As
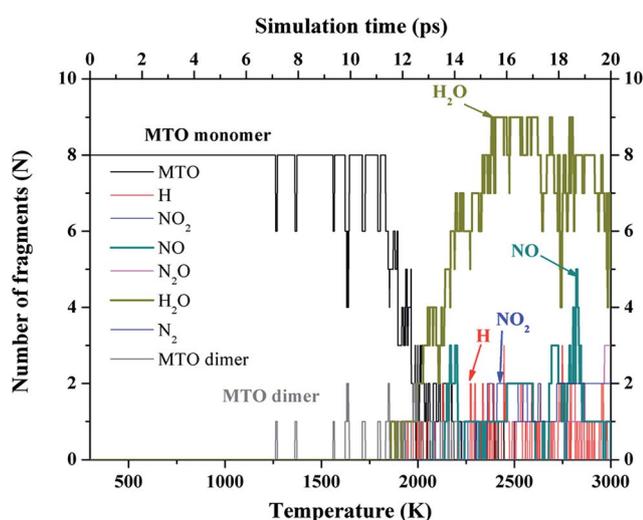
the temperature continues to increase, we observe the release of increased numbers of H_2O products.

3.1.2. Finite cluster calculations.
To understand the nature of the initial decomposition reactions of $P2_{(1)}$-**MTO**, we extracted the activated intermediates from the condensed phase simulation and analyzed the reaction mechanism as a gas phase reaction.

3.1.2a. Intermolecular H transfer to form INT1 (MTO–TS1–INT1). We find that the first reaction is intermolecular hydrogen-transfer in which two **MTO** molecules each exchange one H atom with the other to form the intermediate **INT1** (Fig. 3) *via* **TS1**. This leads to a very low barrier of only $\Delta H = 3.0$ kcal mol^{-1} ($\Delta G = 5.1$ kcal mol^{-1}), which is very fast in the QM-MD above 1250 K. Based on this barrier and we estimate that this should take place in a nanosecond at room temperature, suggesting that the crystallization must be done at low temperature (below 50 K). Although **INT1** has an internal energy of 7.0 kcal mol^{-1}, which is lower than the **TS1** of 7.8 kcal mol^{-1} at zero temperature, we find that at room temperature **INT1** has a higher enthalpy and free energy than the **TS1**.

3.1.2b. Decomposition of INT1′ to release H_2O (INT1′–TS2–INT2 + H_2O). After formation of the **INT1′** (**INT1** monomer) *via* the bimolecular H transfer from **MTO**, we find that one H atom of $–NH_2$ transfers from the N atom to the nearby OH group *via* **TS2** to release one H_2O molecule and **INT2**, with a barrier of $\Delta H = 46.5$ kcal mol^{-1} ($\Delta G = 46.4$ kcal mol^{-1}), making it the rate-determining step (RDS) for decomposition. Indeed this is the first decomposition process we see in the DFT-MD on the periodic system (at $\sim$11.5 ps).

3.1.2c. Decomposition of INT2 to release NO^+ (INT2–TS3–INT3 + NO^+). Starting with **INT2**, the lowest energy pathway to eliminate the NO^+ molecule is to break the C–N bond *via* **TS3** to form an intermediate **INT3** (shown in Fig. 3), which we find to have a barrier of 35.5 kcal mol^{-1} above **INT2**. Indeed we see this process in the DFT-MD on the periodic system at 13 ps.

3.1.2d. MTO get one H^+ from previous decomposed nearby fragments. Between 12.5 and 15.0 ps (2000 K and 2300 K) in the DFT-MD simulations on **MTO** crystal, we found intermediates **INT4**, **INT5** and **INT6** after the first H_2O and NO releasing reaction, (shown in Fig. 4). The mechanism for forming these species is as follows. First, the **MTO** molecule adds a dissociated H^+ from some previous decomposition to the O atom to form the intermediate **INT4**. Then starting from **INT4**, one H atom of $–NH_2$ transfers *via* **TS4** to the nearby OH group to release one H_2O molecule, forming **INT5**. This has a barrier of $\Delta H = 45.4$ kcal mol^{-1} ($\Delta G = 44.4$ kcal mol^{-1}), making it the rate-determining step (RDS) for this decomposition pathway. Then from **INT5** the easiest decomposition pathway is to eliminate the NO^+ molecule by breaking the C–N bond *via* **TS5** to form intermediate **INT6** (shown in Fig. 4), This has a barrier of $\Delta H = 28.2$ kcal mol^{-1} ($\Delta G = 30.3$ kcal mol^{-1}) above **INT5**.

3.1.2e. Intramolecular H transfer (MTO–TS6–INT1′). Although our DFT-MD studies of **MTO** did not find an intramolecular hydrogen-transfer, we carried out QM calculations to examine the barrier for this intramolecular hydrogen-transfer pathway (**MTO–TS6–INT1′**), as shown in Fig. 5. Here one H atom of the $–NH_2$ group transfers to the adjacent O atom to form the
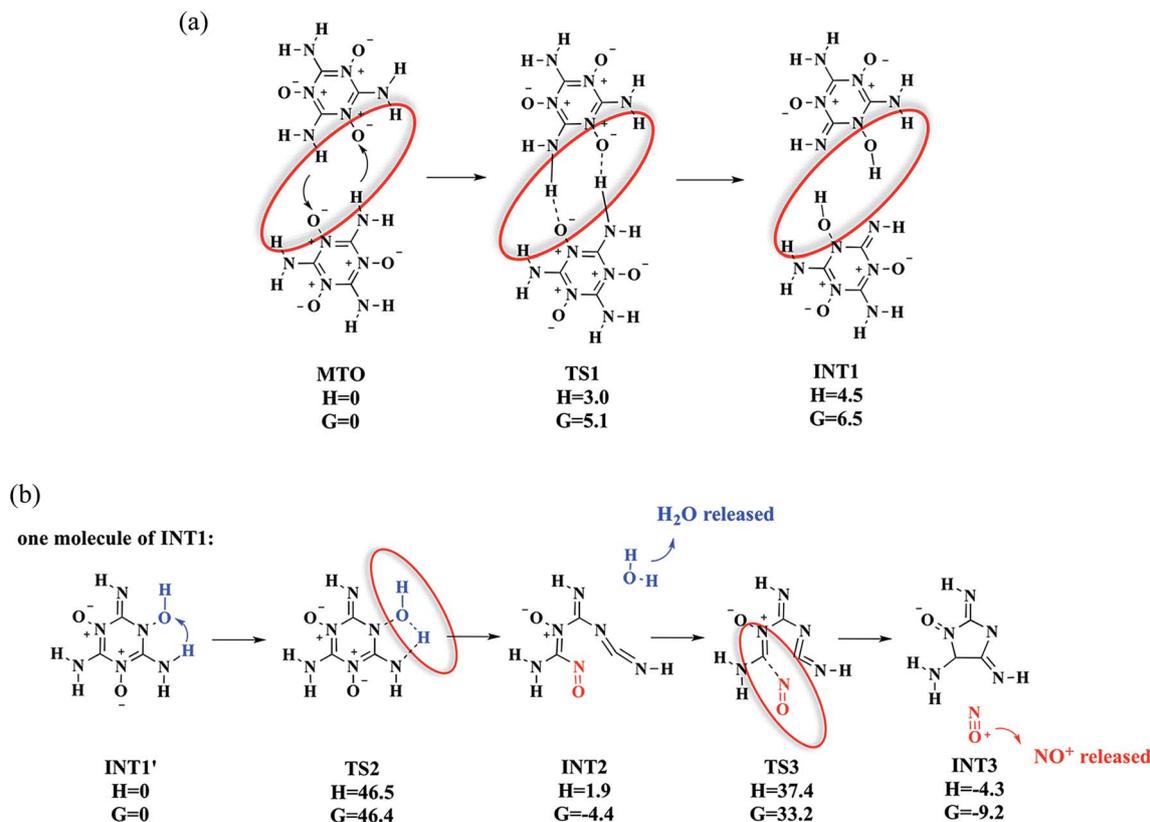

Fig. 2 Species analysis for the decomposition of $P2_{(1)}$-MTO heated from 300 to 3000 K over 20 ps. During 7 to 11 ps, H transfer occurs and at $\sim$11.5 ps ($T = 1800$ K), the first H_2O released. Starting at 13 ps ($\sim$2050 K), one NO molecule is released. The main product of MTO decomposition is H_2O.

12046 | *J. Mater. Chem. A*, 2015, **3**, 12044–12050

This journal is © The Royal Society of Chemistry 2015

Fig. 3 The mechanism of the (a) intermolecular hydrogen-transfer, and (b) H_2O and NO releasing reactions for **MTO**. First a bimolecular intermolecular hydrogen-transfer take place to form **INT1**, then one H_2O is released to form **INT2**, which is followed quickly by NO^+ release to form **INT3**. Configurations **TS1**, **INT1**, **TS2**, **INT2** and **INT3** were extracted from the DFT-MD trajectory and then optimized as a gas phase reaction. We carried out IRC calculations to show that these steps are connected (that is there is no additional TS between **MTO**, **INT1**, **INT2**, and **INT3**). We calculate that the QM energy of the **INT1** is 7.0 kcal mol^{-1} lower than the **TS1** of 7.8 kcal mol^{-1} at 0 K, the **INT1** has a higher enthalpy and free energy at 298.15 K than the **TS1**. Whereas including the hydrogen bonding between the two **INT1'** molecules in **INT1**, the QM energy of the **INT1'** is 4.0 kcal mol^{-1} above the **INT1**. Here energies are in kcal mol^{-1}. The ΔH and ΔG is evaluated at 298.15 K.
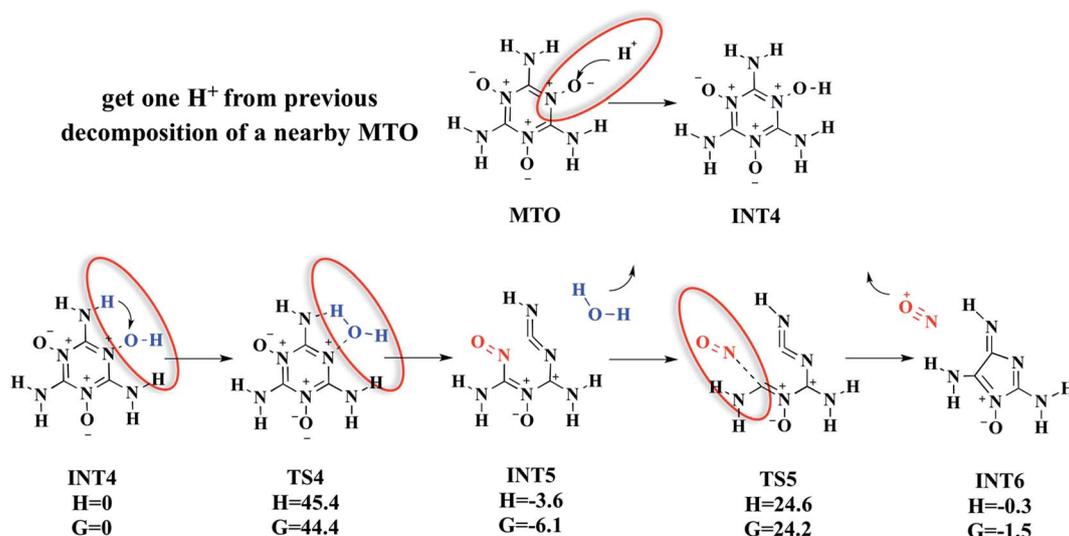

Fig. 4 The mechanism of our proposed pathway for the reactions releasing H_2O and NO^+ from **MTO**, which starts with an H^+ transfer from a previously decomposed **MTO** molecule to an oxygen atom (see the red lines in Fig. 2, which indicate dissociated H atoms) of an unreacted **MTO** to form **INT4**. Then **INT4** releases one H_2O to form **INT5**, which is followed quickly by NO^+ release to form **INT6**. Units are in kcal mol^{-1}.

INT1 *via* **TS6**. This leads to a barrier of $\Delta H = 12.0$ kcal mol^{-1} ($\Delta G = 12.5$ kcal mol^{-1}), which is 9.0 kcal mol^{-1} higher than the simultaneous intermolecular hydrogen-transfer reaction. This explains why we did not observe intramolecular hydrogen-transfer events in the DFT-MD for periodic **MTO**. This pathway would form the same **INT1′** intermediate (one molecule in **INT1**) in the gas phase as shown in Fig. 5. As described above we also found a nearby transition state (**TS6**) with one saddle point and then the nearby stable reactant (**MTO**) and product (**INT1′**) species. Compared with the intermolecular H transfer (discussed above in Fig. 3), the first **INT1** in Fig. 3 has lower energy than **INT1′** in Fig. 5 because of the hydrogen bonding between the two **INT1′** molecules in **INT1** (the hydrogen bond distance is 1.560 Å).

3.2.   MTO3N initial reaction

3.2.1.   Quantum molecular dynamics simulation. For $P2_{(1)}/$c-**MTO3N** the initial decomposition fragments during the cook-off simulation are plotted in Fig. 6 as a function of time (temperature). The starting supercell consists of 8 **MTO3N** molecules (144 atoms).

• From 5 to 12.5 ps, the amplitude of the N–N bond stretching vibration leads to fluctuations beyond our NN cut-off, but no real reactions.

• Then at 12.5 ps ($\sim$2000 K), we observe release of two NO$_2$ molecules simultaneously with three new fragments: **MTO3N–NO$_2$**, **MTO3N–O**, and **MTO3N–NO$_2$ + O** as shown in Fig. 6. Here one NO$_2$ molecule comes from a bimolecular NO$_2$ releasing reaction while the other is from a unimolecular NO$_2$ cleavage reaction.

We will discuss the reaction mechanisms in more detail in the next section using finite cluster calculations. As the temperature continues increasing, we observe release of additional NO$_2$ products.

3.2.2.   Finite cluster calculation. In order to understand the nature of the initial decomposition reactions of $P2_{(1)}/$c-**MTO3N**, we extracted the activated intermediates from the condensed phase simulation and analyzed the reaction mechanism as a gas phase reaction, just as for $P2_{(1)}$-**MTO**. We find that both an initial bimolecular NO$_2$ releasing reaction and a unimolecular NO$_2$ cleavage reaction takes place simultaneously.

The bimolecular NO$_2$ releasing reaction **MTO3N–TS7–INT8** shown in Fig. 7(a) takes place between two **MTO3N** molecules at about 12.5 ps ($\sim$2000 K). In this reaction one oxygen atom of an
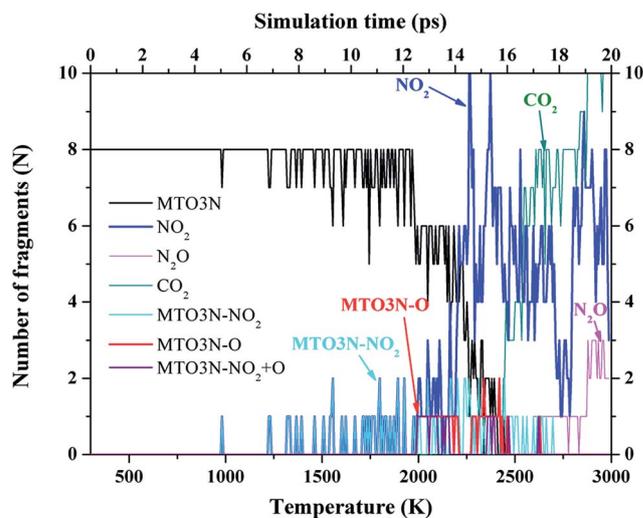

Fig. 6 Species analysis for the decomposition of $P2_{(1)}/$c-**MTO3N** heated from 300 to 3000 K over 20 ps. From 5 to 12.5 ps, we observe only N–N bond stretching vibration (no reactions), and then at 12.5 ps ($\sim$2000 K), we observe release of two NO$_2$ molecules. At the same time, we observe three new fragments (**MTO3N–NO$_2$**, **MTO3N–O**, and **MTO3N–NO$_2$ + O**), which indicate that the two NO$_2$ molecules come both from a bimolecular NO$_2$ releasing reaction and a unimolecular NO$_2$ cleavage reaction. This event is illustrated in Fig. 7.

–NO$_2$ group in **MTO3N** reacts with the carbon atom of the nearby **MTO3N** to make a new C=O double bond *via* **TS7**, accompanied by breaking of the C–N bond, to release one NO$_2$. This bimolecular NO$_2$ releasing reaction (**MTO3N–TS7–INT8**) is the rate-determining step (RDS) with a barrier of $\Delta H = 44.1$ kcal mol^{-1} ($\Delta G = 54.7$ kcal mol^{-1}), which is similar to the barrier of H$_2$O releasing reaction (**INT1′–TS2–INT2**) in **MTO** initial reactions.

Fig. 7(b) shows, the energetics for the unimolecular NO$_2$ cleavage reaction pathway (**MTO3N–INT9**) found in the fragment analysis of Fig. 6 at 12.5 ps ($\sim$2000 K). The reaction barrier (and endothermicity) is calculated to be $\Delta H = 59.9$ kcal mol^{-1} (see Fig. 7(b)), which is 15.8 kcal mol^{-1} higher than the bimolecular NO$_2$ releasing reaction barrier. However the transition state free energy $\Delta G = 58.2$ at 298.15 K is similar to the $\Delta G = 54.7$ for the bimolecular reaction, explaining why the DFT-MD simulation observes both at the same time at 12.5 ps ($\sim$2000 K).
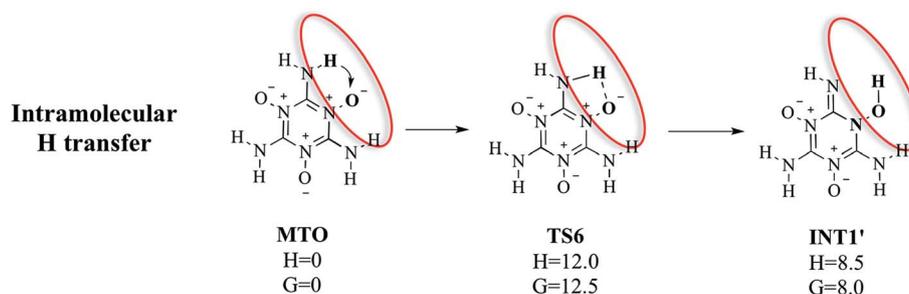

Fig. 5   The reaction mechanism for the intramolecular H transfer path **MTO–TS6–INT1′** that forms one molecule of **INT1**, this path was observed in gas phase but was not observed in the DFT-MD simulations. Here energies are in kcal mol^{-1}.

(a)

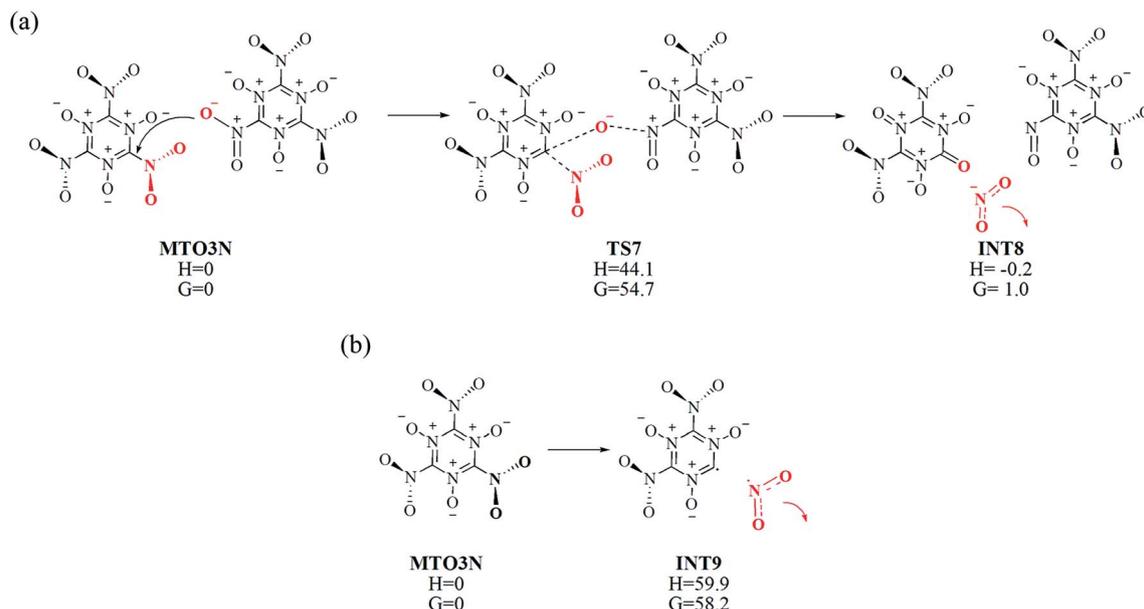**MTO3N**
H=0
G=0

TS7
H=44.1
G=54.7

INT8
H= -0.2
G= 1.0

(b)

MTO3N
H=0
G=0

INT9
H=59.9
G=58.2

Fig. 7 (a) The mechanism of the bimolecular NO_2 releasing reaction **MTO3N–TS7–INT8**, which takes place between two **MTO3N** molecules at 12.5 ps (~2000 K). In this reaction one oxygen atom of the $-NO_2$ group in **MTO3N** reacts with the carbon atom of a nearby **MTO3N** to make a new C=O double bond via **TS7** while displacing the NO_2 from this C atom. (b) The unimolecular NO_2 cleavage reaction for **MTO3N**. **MTO3N–INT9** also takes place at 12.5 ps (~2000 K) Energies in kcal mol^{-1}. This reactions have very different ΔH with (a) much more favorable, but the ΔG at 298.15 K is similar.

To understand why the reaction energy (barrier) for the unimolecular NO_2 cleavage reaction in **MTO3N** is much higher than the barrier of the bimolecular NO_2 releasing reaction, we examined the molecular structure of **MTO3N** in both the gas phase and crystal. We found that optimizing the **MTO3N** molecular structure in the gas phase leads to a structure in which, the planes of the three $-NO_2$ group are all perpendicular to the plane of 6-member ring. However, in the optimized **MTO3N** crystal, the angles between the planes of the $-NO_2$ groups on one **MTO3N** molecule and the plane of 6-member ring are 30°, 60°, and 90°, respectively. Moreover in the **MTO3N** crystal the shortest distance between the oxygen atom of $-NO_2$ and the oxygen atom of nearby C=O group is 2.655 Å, much shorter than in gas phase **MTO3N** (3.274 Å). We conclude that the strong intermolecular repulsive force between $-NO_2$ group and the nearby C=O group makes the bimolecular release of the $-NO_2$ group more favorable in the crystal. In contrast for unimolecular NO_2 cleavage unimolecular NO_2 cleavage in **MTO3N** requires a very long atom transfer process, giving it a very high reaction energy (barrier), but this is favored at high temperature because of the increased entropy from the bond breaking process.

4.   Summary and conclusions

The condensed phase DFT-MD temperature programmed simulations uncover competing unimolecular and bimolecular reactions for the initial thermal decomposition reactions of the **MTO** and **MTO3N** energetic materials. We find that these MD results can be explained in terms reaction pathways on just the

one or two molecules involved. Key points of our simulations are:

(1) For $P2_{(1)}$-**MTO**, the initial reaction is a bimolecular hydrogen-transfer reaction, followed first by H_2O release with ring opening and then by NO^+ release. This intermolecular hydrogen-transfer reaction has a very low barrier of $\Delta H = 3.0$ and $\Delta G = 5.1$ kcal mol^{-1}, suggesting that this reaction may proceed in less than an hour even at 100 K. This could be tested by examining the IR and Raman of the crystalline form to find evidence of both OH and C=N bonds. For the **INT1** species formed after the intermolecular hydrogen transfer reactions, it is now most favorable for intramolecular release of H_2O ($\Delta H = 46.5$ and $\Delta G = 46.4$ kcal mol^{-1}) to form **INT2**. From this **INT2** intermediate, it is favourable ($\Delta H = 35.5$ and $\Delta G = 37.6$ kcal mol^{-1}) to break the C–N bond, to release NO^+ while forming an imidazole ring.

(2) For $P2_{(1)}$/**c-MTO3N**, the bimolecular NO_2 releasing reaction and unimolecular NO_2 cleavage reaction take place simultaneously in the DFT-MD. In the bimolecular NO_2 releasing reaction, one oxygen atom of the $-NO_2$ group in **MTO3N** reacts with the carbon atom of a nearby **MTO3N** to form a new C=O double bond while releasing the NO_2 from this carbon, with a $\Delta H = 44.1$ and $\Delta G = 54.7$ kcal mol^{-1} barrier. The reaction energy (barrier) for the unimolecular NO_2 cleavage is calculated to be $\Delta H = 59.9$ and $\Delta G = 58.2$ kcal mol^{-1} leading to a ΔG just slightly higher than the bimolecular NO_2 releasing reaction.

The predicted initial reaction barriers for **MTO** ($\Delta H = 46.5$ kcal mol^{-1}) and **MTO3N** ($\Delta H = 44.1$ kcal mol^{-1}) are higher than the NO_2 dissociation barrier RDX ($\Delta H = 39.0$ kcal mol^{-1})[8] and for HMX[14] ($\Delta H = 39.8$ kcal mol^{-1}). This suggests that both

crystals should be more thermally stable. However the favourable hydrogen transfer processes in **MTO** may lead to problems with synthesis and crystallization. Thus we recommend **MTO3N** as the more promising material.

We have carried out similar DFT-MD simulations to investigate the initial thermal decomposition reaction of TKX-50 [37] and DTTO,[38] which also have been suggested to be insensitive energetic materials. There we found the first decomposition barrier of TKX-50 (45.1 kcal mol^{-1}) and DTTO (45.9 kcal mol^{-1}), which are similar to the value we find for **MTO** (46.5 kcal mol^{-1}) and **MTO3N** (44.1 kcal mol^{-1}). These high decomposition barriers for **MTO** and **MTO3N** suggest that these newly designed green energetic materials: **MTO** and **MTO3N** would be thermally insensitive.

Conflict of interest

The authors declare no competing financial interest.

Acknowledgements

References

1 M. B. Talawar, R. Sivabalan, T. Mukundan, H. Muthurajan, A. K. Sikder, B. R. Gandhe and A. S. Rao, *J. Hazard. Mater.*, 2009, **161**, 589–607.

2 D. M. Badgujar, M. B. Talawar, S. N. Asthana and P. P. Mahulikar, *J. Hazard. Mater.*, 2008, **151**, 289–305.

3 T. M. Klapötke, personal communication, 2014.

4 S. Naserifar, S. V. Zybin, C.-C. Ye and W. A. Goddard III, 2015, unpublished.

5 M. Arellano and S. Bond, *Rev. Econ. Stud.*, 1991, **58**, 277–297.

6 R. G. Parr and R. G. P. W. Yang, *Density-functional theory of atoms and molecules*, Oxford University Press, 1989.

7 H. Kim, J. M. Choi and W. A. Goddard III, *J. Phys. Chem. Lett.*, 2012, **3**, 360–363.

8 D. Chakraborty, R. P. Muller, S. Dasgupta and W. A. Goddard III, *J. Phys. Chem. A*, 2000, **104**, 2261–2272.

9 N. Umezawa, R. K. Kalia, A. Nakano, P. Vashista and F. Shimojo, *J. Chem. Phys.*, 2007, **126**, 234702.

10 R. A. Fifer, *Fundamentals of Solid-Propellant Combustion*, AIAA, New York, 1984.

11 M. R. Manaa, L. E. Fried, C. F. Melius, M. Elstner and T. Frauenheim, *J. Phys. Chem. A*, 2002, **106**, 9024–9029.

12 S. P. Han, A. C. van Duin, W. A. Goddard III and A. Strachan, *J. Phys. Chem. B*, 2011, **115**, 6534–6540.

13 A. Strachan, E. M. Kober, A. C. van Duin, J. Oxgaard and W. A. Goddard III, *J. Chem. Phys.*, 2005, **122**, 54502.

14 D. Chakraborty, R. P. Muller, S. Dasgupta and W. A. Goddard III, *J. Phys. Chem. A*, 2001, **105**, 1302–1314.

15 S. N. Bulusu, *Chemistry and physics of energetic materials*, Kluwer Academic, Boston Norwell, MA, U.S.A., 1990.

16 C. J. Wu and L. E. Fried, *J. Phys. Chem. A*, 1997, **101**, 8675–8679.

17 K. K. Irikura, *J. Phys. Chem. A*, 2013, **117**, 2233–2241.

18 R. Cohen, Y. Zeiri, E. Wurzberg and R. Kosloff, *J. Phys. Chem. A*, 2007, **111**, 11074–11083.

19 X. F. Chen, J. F. Liu, Z. H. Meng and K. L. Han, *Theor. Chem. Acc.*, 2010, **127**, 327–344.

20 S. Okovytyy, Y. Kholod, M. Qasim, H. Fredrickson and J. Leszczynski, *J. Phys. Chem. A*, 2005, **109**, 2964–2970.

21 D. Chakraborty, R. P. Muller, S. Dasgupta and W. A. Goddard III, *J. Comput.-Aided Mol. Des.*, 2002, **8**, 203–212.

22 B. Wang, D. Wright, D. Cliffel, R. Haglund and S. T. Pantelides, *J. Phys. Chem. A*, 2011, **115**, 8142–8146.

23 D. Furman, R. Kosloff, F. Dubnikova, S. V. Zybin, W. A. Goddard III, N. Rom, B. Hirshberg and Y. Zeiri, *J. Am. Chem. Soc.*, 2014, **136**, 4192–4200.

24 C. A. Mayhew, P. Sulzer, F. Petersson, S. Haidacher, A. Jordan, L. Mark, P. Watts and T. D. Mark, *Int. J. Mass Spectrom.*, 2010, **289**, 58–63.

25 Z. Takats, I. Cotte-Rodriguez, N. Talaty, H. W. Chen and R. G. Cooks, *Chem. Commun.*, 2005, 1950–1952.

26 L. M. Minier, K. R. Brower and J. C. Oxley, *J. Org. Chem.*, 1991, **56**, 3306–3314.

27 L. L. Davis and K. R. Brower, *J. Phys. Chem.*, 1996, **100**, 18775–18783.

28 A. Strachan, A. C. van Duin, D. Chakraborty, S. Dasgupta and W. A. Goddard III, *Phys. Rev. Lett.*, 2003, **91**, 098301.

29 W. Kohn and L. J. Sham, *Phys. Rev.*, 1965, **140**, A1133–A1138.

30 P. Hohenberg and W. Kohn, *Phys. Rev.*, 1964, **136**, B864–B871.

31 G. Kresse, *J. Non-Cryst. Solids*, 1995, **193**, 222–229.

32 G. Kresse and J. Furthmuller, *Comput. Mater. Sci.*, 1996, **6**, 15–50.

33 G. Kresse and J. Furthmuller, *Phys. Rev. B: Condens. Matter Mater. Phys.*, 1996, **54**, 11169–11186.

34 G. Kresse and D. Joubert, *Phys. Rev. B: Condens. Matter Mater. Phys.*, 1999, **59**, 1758–1775.

35 A. D. Bochevarov, E. Harder, T. F. Hughes, J. R. Greenwood, D. A. Braden, D. M. Philipp, D. Rinaldo, M. D. Halls, J. Zhang and R. A. Friesner, *Int. J. Quantum Chem.*, 2013, **113**, 2110–2142.

36 K. Fukui, *Acc. Chem. Res.*, 1981, **14**, 363–368.

37 Q. An, W. Liu, W. A. Goddard III, T. Cheng, S. V. Zybin and H. Xiao, *J. Phys. Chem. C*, 2014, **118**, 27175–27181.

38 C.-C. Ye, Q. An, W. A. Goddard III, T. Cheng, W.-G. Liu, S. V. Zybin and X.-H. Ju, *J. Mater. Chem. A*, 2015, **3**, 1972–1978.